Eur. Phys. J. E (2013) **36**: 112
DOI 10.1140/epje/i2013-13112-2

THE EUROPEAN PHYSICAL JOURNAL E

Regular Article

Forces on a saltating grain in air

Zhen-Ting Wang[1,2,a], Chun-Lai Zhang[1,b], and Hong-Tao Wang[2]

[1] State Key Laboratory of Earth Surface Processes and Resource Ecology, Beijing Normal University, Beijing, 100875, P.R. China
[2] Key Laboratory of Desert and Desertification, Cold and Arid Regions Environmental and Engineering Research Institute, Chinese Academy of Sciences, Lanzhou 730000, P.R. China

Received 25 July 2013 and Received in final form 30 August 2013
Published online: 4 October 2013 –

Abstract. A wind tunnel experiment was performed to measure the trajectories of individual sand grains. Then, the acceleration given by the numerical differentiation was used to assess the relative importance of different external forces on a saltating sand grain in air. It is reconfirmed that the gravitational force and drag are the most important to grain motion. The lift also has certain influence. However, the present research does not support that the electrostatic force is significant.

1 Introduction

The dominant mode of aeolian sand transport is saltation which consists of grains being lifted upwards, traveling downwind and finally colliding with the ground [1]. The characteristics of saltation, including velocity, height, length, liftoff, impact angles, etc., are determined by external forces acting on grains. However, some very different expressions of forces are applied in various saltation models because it is often difficult to directly measure the forces on a moving grain. In the pioneering work of Bagnold [1], only two forces, *i.e.* gravity and drag, were taken into consideration. Thereafter, several other forces, *e.g.* lift, Magnus force, Saffman force and the electrostatic force, were successively introduced [2–10]. The linear superposition of these forces is currently regarded as the resulting force [6,7]. Is such an approach logical? In fact, the forces mentioned above can be classified into field force and aerodynamic force. Gravity and electric force belong to field force. Under the framework of classical mechanics, they are independent variables and satisfy the superposition principle. The aerodynamic force, a reflection of the interaction of sand and airflow, includes the so-called drag, lift, Magnus force, Saffman force, Basset force, etc. The fluid motion can be described by a Navier-Stokes equation accurately. Given a solution or a velocity field, the aerodynamic force is equal to the integral of fluid stress over the surface of the sand grain. Every expression of aerodynamic force corresponds to a certain simplified flow field. For example, the Saffman force on a small sphere moving through a very viscous liquid was derived under the assumption that three Reynolds numbers are small compared with unity [11,12]. The strong non-linearity of the Navier-Stokes equation prevents the linear superposition of all kinds of aerodynamic forces. Therefore, the governing equation of the center of mass of a grain can be written as

$$m\mathbf{a} = m\mathbf{g} + \mathbf{F_e} + \mathbf{F_a}, \tag{1}$$

where m, $\mathbf{a}$, $\mathbf{g}$, $\mathbf{F_e}$, $\mathbf{F_a}$ are mass, acceleration, gravitational acceleration, electric force, and aerodynamic force, respectively.

The purpose of this research is to find the acceleration from the measured trajectory and then investigate the relative importance of different external forces on a saltating grain.

2 Materials and methods

The experiments were performed in a 15.6 m long, 1.0 m wide, and 1.0 m high wind tunnel whose top surface and two sidewalls are made of clear glass. The wind speed with a turbulence intensity less than 0.5% on the axis of the tunnel can be continuously changed from 2 m/s to 45 m/s. The bottom surface of the working section was covered by dry, loose, artificial sand with mean diameter of $d = 800\,\mu$m and a density of $2.65 \times 10^3\,\mathrm{kg/m^3}$. The 8 mm thick sand bed was carefully smoothed by a small uniform pressure. Similar to many previous works [13–15], the saltation trajectories were recorded by a horizontal high-speed camera with the help of an orthogonal 532 nm laser sheet. The frame rate, spatial resolution and exposure time were adjusted to 3000 fps, 1820×720 pixels and

[a] e-mail: wangzht@lzu.edu.cn
[b] e-mail: clzhang@bnu.edu.cn

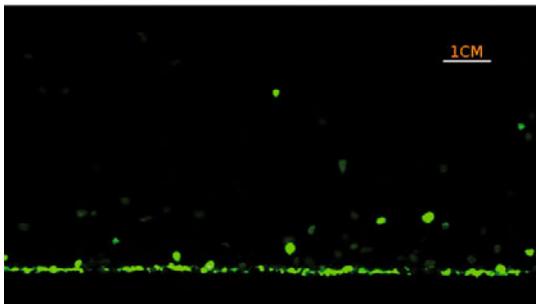

Fig. 1. (Color online) a typical raw image recorded by the high-speed camera.

1/3000 s, respectively. The wind speed profile was measured with a series of Pitot tubes at different heights. All experiments were conducted at night and the relative environmental factors, such as temperature and humidity, did not change significantly.

Figure 1 is a typical raw image recorded by the high-speed camera. Because of coarse sand, strong laser intensity, and the powerful high-speed camera, single saltating grains could be easily distinguished. For more accuracy, an image process was developed [16]: the disturbances obtained by averaging a large number of recordings [13] were firstly eliminated; then the binary images were given by Otsu's method [17] and a simply connected region with the area larger than 9 pixels was recognized as a grain; finally, the position of a grain at the next instant was determined by comparing its area with the "neighbors" in the next image.

Numerical differentiation is a well-known ill-posed problem. Small pertubations in the obtained trajectory of saltation may lead to large errors in the computed acceleration. To date, a number of techniques have been developed [18–21]. Difference, interpolation, and regularization are three common methods [22]. Here we select a powerful regularization method in which a quadratic term is used for the regularization [23].

After calculating the acceleration $\mathbf{a}$, field force $\mathbf{F_e}$ and aerodynamic force $\mathbf{F_a}$ can be assessed on a quantitative basis. We choose the right-handed coordinate system such that the wind direction is x, the direction perpendicular to the sand bed is z and the transverse direction is y. The limited measurements of electric fields and grain charges in the saltation indicates that the x and y components of the electrostatic field are negligible [6,7,24]. Thus, $\mathbf{F_e}$ only has a vertical component

$$F_{ez} = mC_eE_z, \tag{2}$$

where C_e and E_z are the charge per unit mass and the field intensity.

The aerodynamic force is usually decomposed into the drag force $\mathbf{F_d}$ in the direction of the relative motion and the orthogonal lift force $\mathbf{F_l}$ [25,26]. $\mathbf{F_d}$ can be written as

$$\mathbf{F_d} = -\frac{1}{2}C_d\rho_a A\mathbf{u_r}|\mathbf{u_r}|, \tag{3}$$

where C_d is the drag coefficient, ρ_a is the air density, A is the front face area, $\mathbf{u_r}$ is the grain-wind relative velocity.

A good empirical formula of C_d is [27]

$$C_d = \frac{24}{Re}(1+0.27Re)^{0.43} + 0.47[1-\exp(-0.04Re^{0.38})], \tag{4}$$

in which the Reynolds number $Re = \frac{\rho_a|\mathbf{u_r}|d}{\mu}$, where d is the grain diameter, μ is the dynamic viscosity of air.

Analogously, the expression of $\mathbf{F_l}$ is

$$\mathbf{F_l} = \frac{1}{2}C_l\rho_a A|\mathbf{u_r}|^2, \tag{5}$$

where C_l is the lift coefficient. $\mathbf{F_l}$ is sometimes called the Magnus force because C_l is often related to the dimensionless rotational velocity $\gamma = \frac{\Omega d}{2|\mathbf{u_r}|}$, where Ω is the angular velocity. A complicated but valid correlation of C_l is the following [28],

$$C_l = \frac{24}{Re^{0.3}} \times \begin{cases} \frac{0.8\gamma(\gamma-\gamma_0)}{\gamma_0} & \text{if } \gamma < \gamma_0, \\ -\frac{a_1(\gamma-\gamma_0)(\gamma+\gamma_0+a_2-2\gamma_1)}{(\gamma_1-\gamma_0)(\gamma_1-\gamma_0-a_2)} & \text{if } \gamma_0 < \gamma < \gamma_1, \\ (a_1-a_3)\exp\left(\frac{\gamma-\gamma_1}{a_4}\right)\cos\left(\frac{2\pi(\gamma-\gamma_1)}{a_5}\right) & \\ \quad + a_2(\gamma-\gamma_1)+a_3 & \text{if } \gamma > \gamma_1, \end{cases} \tag{6}$$

where $\gamma_0 = -0.125(\frac{Re}{10^4}-8)(\frac{Re}{10^4}-12)$ (if $8\times10^4 < Re < 1.2\times10^5$) or zero (otherwise), $\gamma_1 = \frac{11}{Re^{0.15}}$, $a_1 = 0.14Re^{0.1}$, $a_2 = \frac{180}{Re}$, $a_3 = 0.12Re^{0.11}$, $a_4 = \frac{20.023}{Re^{0.3}}$, $a_5 = \frac{1800}{Re^{0.6}}$.

Equation (5) determines the magnitude of $\mathbf{F_l}$. As a vector, it is parallel to $\mathbf{\Omega}\times\mathbf{u_r}$. In wind tunnel experiments, it is impossible to simultaneously measure the three components of $\mathbf{\Omega}$ using one high-speed camera. Because the flow field is axisymmetric about the centreline (x-axis) of the wind tunnel and the wind speed increases with height, there exists one situation in which $\boldsymbol{\Omega} = \omega\mathbf{j}$, where $\mathbf{j}$ is the unit vector in the y-direction. ω can be reliably obtained by tracking special speckles on the grain surface or the position of the prolate axis of irregular grain [29,30].

Substituting eqs. (2), (3), (5) into eq. (1) and noting that $\boldsymbol{\Omega} = \omega\mathbf{j}$, $m = \frac{1}{6}\rho_s\pi d^3$, and $A = \frac{1}{4}\pi d^2$, we have

$$a_x = \frac{3}{4}\frac{\rho_a}{\rho_s}\sqrt{(v_x-U)^2+v_z^2}\left(-C_d\frac{v_x-U}{d}+C_l\frac{v_z}{d}\right), \tag{7a}$$

$$a_z = -g + C_eE_z - \frac{3}{4}\frac{\rho_a}{\rho_s}\sqrt{(v_x-U)^2+v_z^2} \times\left(C_d\frac{v_z}{d}+C_l\frac{v_x-U}{d}\right), \tag{7b}$$

where ρ_s is the density of sand, v_x and v_z are two velocity components of the grain, U is the wind speed. Given the measured time series of a trajectory, the first and second derivatives of the displacement with respect to time are the velocity $\mathbf{v}$ and the acceleration $\mathbf{a}$, respectively. The mathematical objective of this numerical differentiation

process is to find an optimal function to minimize the sum of a goodness-of-fit term and a regularization term, see ref. [23] for the detailed general concepts, algebra formalism and method of choosing the regularization parameter.

Neglecting the effects of temporal turbulent fluctuations, the vertical profile of wind speed is given by a logarithmic law

$$U = \frac{u_*}{\kappa} \log\left(\frac{z}{z_{0s}}\right), \tag{8}$$

where u_*, $\kappa(= 0.4)$ and z_{0s} are the friction velocity, Kármán's constant, and the aerodynamic roughness, respectively. u_* was estimated by using the wind speeds above the saltation layer. There are some theoretical or empirical expressions of z_{0s} [31–33]. For simplicity, z_{0s}, approximately ranging from $\frac{d}{30}$ to $\frac{d}{10}$ here, was treated as a fitting parameter of the measured data. The fitted profile of wind speed is less precise at a height very close to the sand bed.

For convenience, we introduce $\mathbf{a_d}$ and $\mathbf{a_l}$ to represent the contributions of $\mathbf{F_d}$ and $\mathbf{F_l}$. Their components are

$$a_{dx} = -\frac{3}{4} C_d \frac{\rho_a}{\rho_s} \frac{v_x - U}{d} \sqrt{(v_x - U)^2 + v_z^2}, \tag{9a}$$

$$a_{dz} = -\frac{3}{4} C_d \frac{\rho_a}{\rho_s} \frac{v_z}{d} \sqrt{(v_x - U)^2 + v_z^2}, \tag{9b}$$

$$a_{lx} = \frac{3}{4} C_l \frac{\rho_a}{\rho_s} \frac{v_z}{d} \sqrt{(v_x - U)^2 + v_z^2}, \tag{9c}$$

$$a_{lz} = -\frac{3}{4} C_l \frac{\rho_a}{\rho_s} \frac{v_x - U}{d} \sqrt{(v_x - U)^2 + v_z^2}, \tag{9d}$$

Then, eq. (7) can be rewritten as

$$a_x = a_{dx} + a_{lx}, \tag{10a}$$

$$a_z = -g + C_e E_z + a_{dz} + a_{lz}. \tag{10b}$$

In the following text, a_x and a_z will denote two acceleration components directly obtained from the experimental data and the right-hand side of eq. (10) will be evaluated.

3 Results and discussions

A total of 120 grains with $\boldsymbol{\Omega} = \omega \mathbf{j}$ were tracked in two wind conditions, $u_* = 0.67\,\mathrm{m/s}$ and $u_* = 0.88\,\mathrm{m/s}$, respectively. The whole trajectory was seldom obtained because the image of sand grains was amplified as large as possible in order to investigate the rotational motion in detail. But a incomplete trajectory will not influence the exploration of various external forces.

Figure 2(a) shows a trajectory in the wind condition of u_*. Different from the assumed constant value in many previous studies, the real angular velocity always changes with time, as shown in fig. 2(b). Figure 3 gives the computed accelerations in this situation. Compared with a_{dx} and a_x, a_{lx} is small enough. The horizontal acceleration

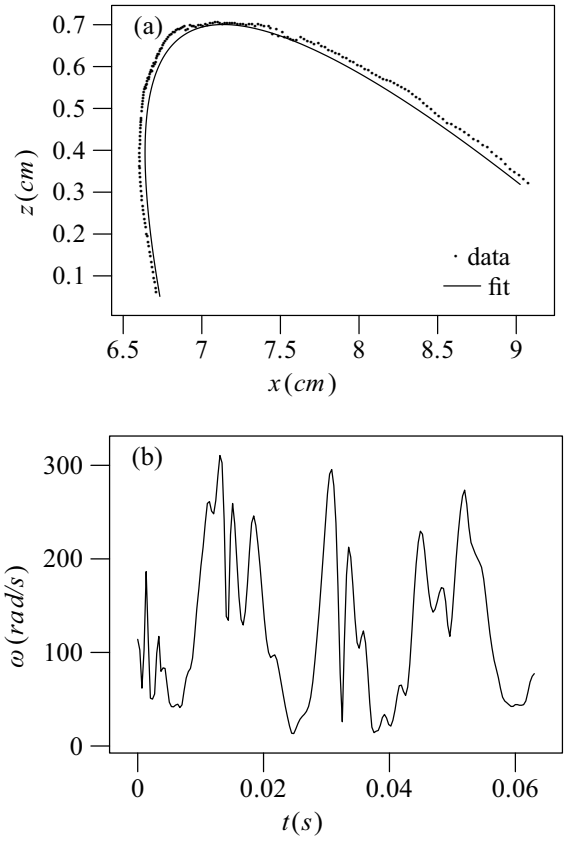

Fig. 2. The dynamic characteristics of saltation, $u_* = 0.67\,\mathrm{m/s}$. (a) The measured trajectory. (b) Change of rotation speed with time.

a_x varies with time t slightly. Therefore, a straight line in fig. 3(a) appears. It is not surprising that $a_{dx} \approx a_x$ while sand grains were transported downwind. The relative error of their time-averaged values $|\frac{\overline{a_x} - \overline{a_{dx}}}{\overline{a_x}}|$ is only 6.3% in fig. 3(a). In the vertical direction, the effect of the lift force emerges. a_{lz} is generally less than 10% of a_{dz}. A recent numerical work also indicates that the lift force is of the order of 1% of the drag force [24]. As pointed out by Kok and Renno [34], the inappropriate expression of C_l will cause the overestimation of F_l easily in some previous studies. As more special experiments on the Robins-Magnus effect over the entire ranges of Re and γ are performed, F_l will be computed more accurately. Some authors argued that the electrostatic force plays a significant role [4, 5]. Although the electric phenomenon in sandstorms has been observed for a long time [35], the charging mechanism for sand grains remains to be revealed. At least six potential mechanisms, such as polarization by the atmospheric electric field, contact electrification, triboelectrification, piezoelectrification, etc., were suggested [36]. The transferring process of electrons is crucial to the charging mechanism for sand grains. It is experimentally and theoretically demonstrated that electrons can be transferred from larger to smaller dielectric grains which are chemically identical [37]. In the strong electric field, identical dielectric grains could be polarized and the electrons trans-

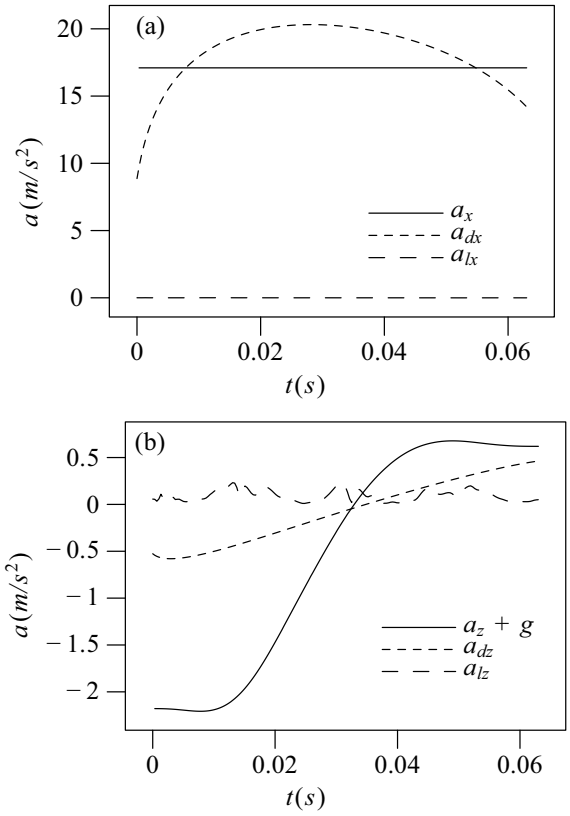

Fig. 3. Change of acceleration with time, $u_* = 0.67\,\mathrm{m/s}$. (a) x-component. (b) z-component.

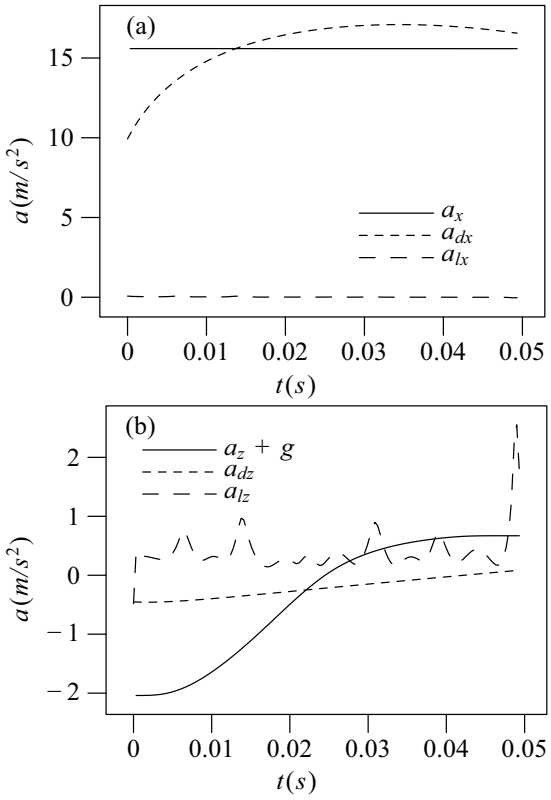

Fig. 5. Change of acceleration with time, $u_* = 0.88\,\mathrm{m/s}$. (a) x-component. (b) z-component.

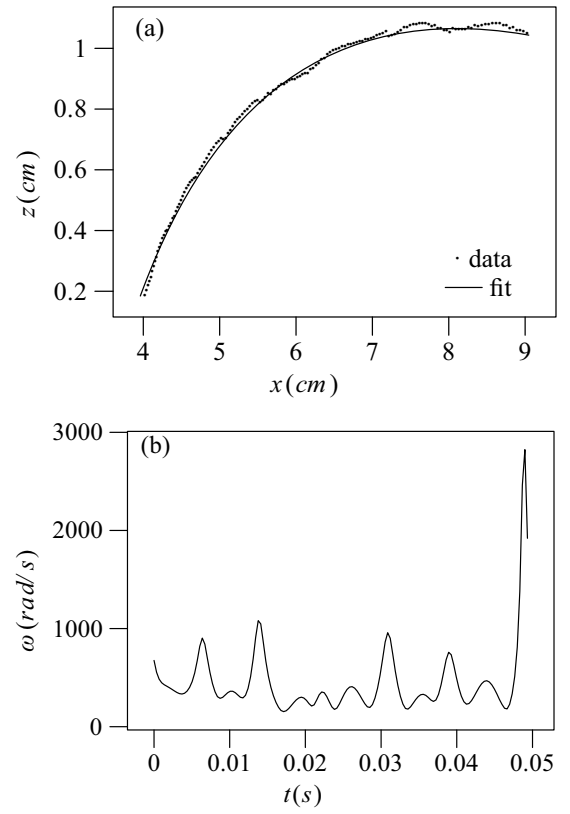

Fig. 4. The dynamic characteristics of saltation, $u_* = 0.88\,\mathrm{m/s}$. (a) The measured trajectory. (b) Change of rotation speed with time.

fer due to the repeated collisions are expected [38]. Sand grains could also be charged by capturing and attracting the ions in their environment. Quartz is the most well-known piezoelectric material. Does the mechanical stress generated in frictions or collisions between sand grans lead to the electric charge separation? The physical mechanism behind the electrification of sand is an interesting topic and further studies, *e.g.* the direct measurement of the electric charges on individual grains in the field, are required. According to the limited measurements, $|C_e E_z|$ in eq. (10b) was previously estimated as $\frac{3}{5}g$ [6] or g [4]. However, the present work shows that $|a_z + g|$ is generally no more than $\frac{1}{3}g$. In our opinion, the influence of the electrostatic force on the near surface saltation can be completely neglected in the absence of dust-storm. As for the difference between $a_z + g$ and a_{dz}, their small values and the regularization method of numerical differentiation could lead to such an error.

Figures 4 and 5 show an upward trajectory and its acceleration in the wind condition of $u_* = 0.88\,\mathrm{m/s}$. It is worth noting that a_{lz} is not always close to zero, see fig. 5(b) for detail. In addition to the numerical values of different forces, the computed trajectories provide a vivid comparison. Figure 6 gives three saltation trajectories and their origins. The saltation motion equations, only including the external forces of the horizontal drag and the vertical gravitation, can cause the satisfying trajectory. If the

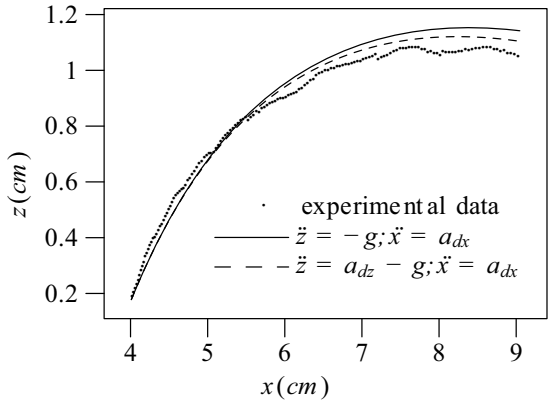

Fig. 6. Comparison of the computed and measured saltation trajectories.

vertical drag is further considered, the computed trajectory will become more accurate, see the dashed line in fig. 6. It is suggested that the analogous governing equations in some saltation models, *e.g.* [39,40], are practical and plausible.

4 Conclusions

The acceleration obtained from the trajectory by the numerical regularization method provides a reliable approach to assess the relative importance of different external forces on a saltating grain in the aeolian transport process of sand. It is reconfirmed that the gravitational force and drag are the most important to grain motion. For some unknown ranges of Reynolds number and the dimensionless rotational velocity, the lift has certain influence on saltation. It seems that the electrostatic force is insignificant.

The authors are grateful to Na Zhou and Li-Qiang Kang for assistance with experimental measurements, to Xue-Yong Zou and Jia-Wu Zhang for helpful suggestions. Thanks go to two anonymous referees for their constructive comments. This research was supported by NSFC project (No. 11274002) and State Key Laboratory of Earth Surface Processes and Resource Ecology project (No. 2013-KF-03).

References

1. R.A. Bagnold, *The Physics of Blown Sand and Desert Dunes* (Chapman and Hall, Methuen, London, 1941), pp. 96-106.
2. B.R. White, J.C. Schultz, J. Fluid Mech. **81**, 497 (1977).
3. B.R. White, Encycl. Fluid Mech. **4**, 239 (1986).
4. D.S. Schmidt, R.A. Schmidt, J.D. Dent, J. Geophys. Res. Atmospheres **103**, 8997 (1998).
5. X. Zheng, N. Huang, Y. Zhou, J. Geophys. Res. Atmospheres **108**, 4322 (2003).
6. Y. Shao, *Physics and Modelling of Wind Erosion* (Springer-Verlag, Berlin, Heidelberg, 2008), pp. 117-210.
7. X. Zheng, *Mechanics of Wind-blown Sand Movements* (Springer-Verlag, Berlin, Heidelberg, 2009), pp. 133-180.
8. N. Huang, C. Wang, X. Pan, J. Geophys. Res. Atmospheres **115**, D22211 (2010).
9. D. Tong, N. Huang, J. Geophys. Res. Atmospheres **117**, D16205 (2012).
10. J.P. Merrison, Aeolian Res. **4**, 1 (2012).
11. P.G. Saffman, J. Fluid Mech. **22**, 385 (1965).
12. P.G. Saffman, J. Fluid Mech. **31**, 624 (1968).
13. W. Zhang, J.-H. Kang, S.-J. Lee, Geomorphology **86**, 320 (2007).
14. W. Zhang, J.-H. Kang, S.-J. Lee, J. Visual. **10**, 39 (2007).
15. T.D. Ho, A. Valance, P. Dupont, A.O.E. Moctar, Phys. Rev. Lett. **106**, 094501 (2011).
16. Z-.T. Wang, Q.-H. Zhang, Z.-B. Dong, Sci. Cold Arid Regions **3**, 13 (2011).
17. N. Otsu, IEEE Trans. System Man Cybern. **SMC-9**, 62 (1979).
18. A. Spitzbart, N. Macon, Am. Math. Month. **64**, 721 (1957).
19. J. Cullum, SIAM J. Num. Anal. **8**, 254 (1971).
20. R. Chartrand, Numerical differentiation of noisy, nonsmooth data, Technical report LA-UR-05-9309 (Los Alamos National Laboratory, 2005).
21. S. Lu, S.V. Pereverzev, Math. Comput. **75**, 1853 (2006).
22. I. Knowles, R. Wallace, Numer. Math. **70**, 91 (1995).
23. J.J. Stickel, Comput. Chem. Engin. **34**, 467 (2010).
24. J.F. Kok, E.J.R. Parteli, T.I. Michaels, D.B. Karam, Rep. Prog. Phys. **75**, 106901 (2012).
25. B. Oesterlé, T.B. Dinh, Exp. Fluids **25**, 16 (1998).
26. N. Lukerchenko, Y. Kvurt, I. Keita, Z. Chara, P. Vlasak, Particulate Sci. Technol. **30**, 55 (2012).
27. N.-S. Cheng, Powder Technol. **189**, 395 (2009).
28. S.M. Persson, Aerodynamic Forces on a Sphere under General Motion - Literature Review and Developments. Technical Report (Aerospace Mechatronics Laboratory, McGill University, Canada, 2007).
29. X. Wu, Q. Wang, Z. Luo, M. Fang, K. Cen, Powder Technol. **181**, 21 (2008).
30. Q. Zhang, Int. J. Land Proc. Arid Environ. **1**, 15 (2012).
31. D.J. Sherman, Geomorphology **5**, 419 (1992).
32. D.J. Sherman, E.J. Farrell, J. Geophys. Res. **113**, F02S08 (2008).
33. O. Durán, H. Herrmann, J. Stat. Mech. Theory and Experiment **07011**, (2006).
34. J.F. Kok, N.O. Renno, J. Geophys. Res. Atmospheres **114**, D17204 (2009).
35. J. Latham, J. R. Meteorol. Soc. **90**, 91 (1961).
36. S.P. Kanagy II, C.J. Mann, Earth-Science Rev. **36**, 181 (1994).
37. J.F. Kok, D.J. Lacks, Phys. Rev. E **79**, 051304 (2009).
38. T. Pähtz, H.J. Herrmann, T. Shinbrot, Nat. Phys. **6**, 364 (2010).
39. M.P. Almeida, J.S. Andrade Jr, H.J. Herrmann, Eur. Phys. J. E **22**, 195 (2007).
40. M.V. Carneiro, N.A.M. Araújo, T. Pähtz, H.J. Herrmann, Phys. Rev. Lett. **111**, 058001 (2013).